Ammonia-Promoted Rhenium-Cluster Formation in CH_3ReO_3-Encapsulated H-ZSM-5 Relevant to the Performance of the Catalytically Selective Oxidation/Ammoxidation of Propene

Nagabhatla Viswanadham,† Takafumi Shido, Takehiko Sasaki, and Yasuhiro Iwasawa*

Department of Chemistry, Graduate School of Science, The University of Tokyo, Hongo, Bunkyo-ku, Tokyo 113-0033, Japan

Received: March 21, 2002; In Final Form: July 16, 2002

HZcvd catalysts, which were prepared by chemical vapor deposition (CVD) of methyl trioxorhenium CH_3ReO_3 on H-ZSM-5 (HZ) and subsequent treatment at 673 K, exhibited significant activities in the selective oxidation/ammoxidation of propene. The catalytic selective oxidation of propene to acrolein never proceeded in the absence of ammonia. In the HZcvd catalysts, the hydrophilic nature of HZ increased, and the crystallinity of the HZ framework decreased as indicated by XRD. The detailed characterizations by XRD, ^{29}Si and ^{27}Al MAS NMR, XANES, and EXAFS at the sequential stages of the catalyst preparation demonstrated the occurrence of structural changes of Re species during the preparation and under the catalytic reaction conditions. CH_3ReO_3 interacted with protons of HZ at 333 K, the subsequent treatment at 673 K formed tetrahedral [ReO_4] monomer, and ammonia promoted the formation of a new [Re_6O_{17}] cluster at 673 K. A proposed cluster structure constituted an octahedral Re_6 framework with an Re−Re bond at 0.276 nm and terminal and bridge oxygen atoms (Re═O at 0.172 nm and Re−O at 0.203 nm, respectively). Thirty-two percent of these oxygen atoms were active for the selective oxidation of propene to acrolein. The active [Re_6O_{17}] clusters were converted to the inactive [ReO_4] monomers in the absence of ammonia.

1. Introduction

Selective oxidation/ammoxidation of light hydrocarbons is one of the most important reactions in both fundamental research and industrial process. Catalysts used for these reactions are multicomponent metal oxides with V or Mo oxide as a main active component.[1−15] W, Nb, and Fe have also often been used as active elements.[10,16−19] Rhenium is another important metal that has been extensively used as a vital catalyst component for several hydrocarbon conversion processes such as reforming, alkene metathesis, and hydrodesulfurization of crude-oil fractions.[20−24] For these reactions, the performance of Re catalysts is superior to that of Mo and V catalysts. Zeolite-supported metallic Re catalysts have also been reported to be efficient catalysts for the conversion of methane to benzene and hydrogen.[25,26] Because of its variable valence, ReO_x supported on oxides catalyzes selective oxidation reactions such as the oxidation of methanol and ethanol to aldehydes and the oxidation−dehydration of methanol to methylal.[20,21,27−31] A crystalline mixed oxide $SbRe_2O_6$ was found to be active for the catalytic selective ammoxidation of iobutylene and isobutane to methacrolein.[32−37] As seen in the literature, limited applications of supported Re oxides to the selective oxidation/ammoxidation of light hydrocarbons have been reported so far. Recently, we have found that a ReO_x/zeolite system (HZcvd) prepared by a chemical vapor deposition (CVD) of CH_3ReO_3 (MTO) on H-ZSM-5 (HZ) and subsequent treatment at 673 K can be a promising candidate for the catalytic selective oxidation/ammoxidation of propene.[38] However, the reason for the best performance of HZcvd among all ReO_x/zeolite catalysts examined was not clear. It was reported that in a MTO/HY metathesis catalyst the MTO molecules retained the structure,[39] but the chemistry of the MTO in the HZcvd catalyst should be much different from that in the metathesis catalyst because the treatment temperature for HZcvd was much higher than that for the MTO decomposition. Furthermore, the existence of ammonia was a prerequisite to the performance of the HZcvd catalyst for the catalytic selective oxidation of propene, but the reason is not clear.

The present study is aimed at the characterization of the selective oxidation/ammoxidation performance of the HZcvd catalyst, the important role of ammonia in the catalytic performance, and the active ReO_x structure by means of XRD, ^{29}Si and ^{27}Al MAS NMR, XANES, and EXAFS. We have found the increase in the hydrophilic nature and the decrease in the crystallinity of the HZ framework by Re incorporation into HZ and the formation of a novel [Re_6O_{17}] cluster under the catalytic reaction conditions in the presence of ammonia.

2. Experimental Section

2.1. Catalyst Preparation. Preparations of various ReOx/zeolite catalysts by CVD, incipient wetness impregnation, and physical mixing methods have been reported in the previous paper, but they are briefly described below.[38] Three zeolites (Mobil Oil Corporation)—HZSM-5 (Si/Al = 39), NaZSM-5 (Si/Al = 39), and HY (ultrastable form with Si/Al = 39.4)—were employed as supports for ReO_x species. To compare the catalytic activities of the ReO_x/zeolite catalysts, rhenium loadings were taken to be about 10 wt %, but low Re-loading samples were also prepared to examine the effect of the Re quantity on the catalytic performance. The exact amounts of Re contained in

* Corresponding author. E-mail: iwasawa@chem..s.u-tokyo.ac.jp. Fax: +81-3-5800-6892.

† Permanent address: Catalysis and Conversion Processes Area, Indian Institute of Petroleum, Dehradun 248005, India.

10.1021/jp020769t CCC: $22.00
Published on Web 09/26/2002

the final catalysts were determined by X-ray fluorescence (XRF). All of the samples were pretreated at 673 K for 4 h under He before use as catalysts.

2.1.1. CVD. Methyl trioxorhenium CH_3ReO_3 (MTO) (99.9% purity, Strem Chemicals) was placed in a glass tube connected to a CVD chamber, and the whole system was evacuated to 10^{-3} Pa. A given amount of MTO was heated at 333 K for its sublimation, and the vapor was allowed to enter the chamber where the zeolites were pretreated in situ at 673 K for 4 h under vacuum (10^{-3} Pa). After MTO adsorption in zeolite pores for typically 14 h at room temperature (RT), the samples were evacuated at RT to remove undeposited MTO. The samples are denoted as HZmto and NaZmto for HZSM-5 (HZ) and NaZSM-5 (NaZ), respectively. HZmto and NaZmto were treated at 673 K for 4 h in a He flow before use as catalysts. These catalysts are denoted as HZcvd and NaZcvd, respectively.

2.1.2. Incipient Wetness Impregnation. A given amount of NH_4ReO_4 (>99.9% purity, Strem Chemicals) was dissolved into 10 mL of deionized water to which a given amount of the zeolite (HZ or HY) was added with constant stirring. The obtained slurry was heated on a water bath to remove the water, followed by drying the sample overnight at RT and then heating at 373 K for 4 h. The samples were further treated at 673 K for 4 h in a He flow before use as catalysts. The samples then obtained are denoted as HZimp and HYimp, respectively.

2.1.3. Physical Mixing. A given amount of NH_4ReO_4 was ground well with a given amount of HZ, and the resultant mixture was heated at 373 K for 4 h to remove ammonia, followed by treatment at 673 K for 4 h in a He flow before use as a catalyst. The sample is denoted as HZphy.

2.2. Characterization. The samples were characterized by X-ray fluorescence spectroscopy (XRF), X-ray diffraction (XRD), solid-state ^{29}Si MAS NMR, solid-state ^{27}Al MAS NMR spectroscopy, FTIR, and X-ray absorption fine structure (XAFS). Special attention was given to understand the structural changes of the Re species in HZ after sequential treatments and catalytic reaction.

2.2.1. XRD. XRD measurements in air were conducted on a Rigaku Miniflex goniometer in a continuous $\theta/2\theta$ scan reflection mode using Cu Kα radiation ($\lambda = 1.5418$ Å). The anode was operated at 30 kV and 15 mA, and the 2θ angles were scanned from 5 to 70° at a rate of 1° min^{-1}.

2.2.2. Solid-State MAS NMR. Solid-state magic-angle spinning (MAS) ^{29}Si NMR spectra were recorded on a Chemagnetics CMX-300 spectrometer using zirconia rotors of 5-mm diameter spinning at 3.5 kHz in air. The spectra were acquired at 59.68 MHz by cross polarization (CP) with a 90° pulse, where the contact time was 4 ms and the pulse delay was 5 s. The 3000 scans gave good spectra. Chemical shifts (ppm) are referenced to an external polydimethylsilane (PDMS) standard. The Si/Al ratios $(Si/Al)_F$ of the zeolite framework were determined from the well-known equation[40]

$$(Si/Al)_F = \frac{\sum_{n=0}^{4} I\mathrm{Si}(n\mathrm{Al})}{\sum_{n=0}^{4} 0.25nI\mathrm{Si}(n\ \mathrm{Al})}$$

where I is the peak intensity and n is an integer (1−4) that describes the number of Al atoms associated with Si.

Solid-state ^{27}Al MAS NMR spectra were recorded with 78.2-MHz spinning frequencies at a pulse length of 1 μs, which corresponds to a $\pi/12$ pulse for nonselective excitation.

2.2.3. XAFS. XAFS spectra were measured at BL-9A and 12C stations of the Photon Factory, the Institute of Materials Structure Science, High Energy Accelerator Research Organization (KEK-IMSS-PF). The energy and current of electrons in the storage ring were 2.5 GeV and 250−400 mA, respectively. X-rays from the storage ring were monochromatized by Si(111) double crystals and were focused by Rh-coated bent cylindrical mirrors. The threshold energies of the mirrors were 23 and 15 keV, respectively, at BL-12C and BL-9A so that the higher harmonics were rejected by the mirrors. Ionization chambers filled with pure N_2 and Ar/N_2 (50/50) mixed gas were used to monitor the incident and transmitted X-rays, respectively. Re L_{III}- and L_I-edge XAFS spectra were measured in a transmission mode at 10 K. The samples were transferred from a Schlenk tube to XAFS cells in a glovebox, which were sealed with wax without exposure to air. The sample thickness was regulated so that the total X-ray absorbance was less than 3. EXAFS spectra were analyzed by the UWXAFS package.[41] The phase shift and amplitude functions were calculated by the FEFF8 code.[42] The threshold energy E_0 was tentatively set at the inflection point of the absorption edge. The k^3-weighted EXAFS oscillation was Fourier transformed into R space. The curve fitting analysis was carried out using the FEFFIT program in R space. The k range for the Fourier transformation and fitting R range were 30−140 nm^{-1} and 0.1−0.32 nm, respectively. The fitted parameters were coordination numbers (CN), interatomic distances (R), Debye−Waller factors (σ), and a correction to the edge energy (ΔE_0). The same ΔE_0 was used for all of the shells.

2.3. Catalytic Performance. The selective oxidation/ammoxidation reactions of propene were carried out in a fixed-bed down-flow reactor made from Pyrex glass (6-mm diameter) at atmospheric pressure using 100 mg of the catalyst (mesh 400 μm). In a typical experimental procedure, the MTO−CVD catalysts were pretreated at 673 K for 4 h under a He flow of 32 mL/min. Then the reactant feed of a mixture of propene, ammonia, oxygen, and helium (7.5%, 7.5%, 10.0%, and 75.0%, respectively) was introduced into the reactor at 673 K at a flow rate of 32 mL/min, which corresponds to a gas hourly space velocity (GHSV) of 19 200 h^{-1}, measured by digital mass-flow controllers. The outlet stream line from the reactor to a gas chromatograph was heated at 393 K to avoid the condensation of reaction products. The reactants and products were analyzed by a gas chromatograph using two columns: Gaskuropack for hydrocarbons and Carboxen for CO_2. The conversion and selectivity were calculated on the basis of the carbon number of the components and are defined by

$$\text{selectivity (C\%)} = (\text{products/consumed propene}) \times 100$$

$$\text{yield (\%)} = \text{conversion} \times \text{selectivity}$$

From a blank test conducted in an empty reactor, we ascertained that no reaction occurred under the present reaction conditions. The performance of various ReO_x/zeolite catalysts in the propene oxidation/ammoxidation was examined at 673 K, and the HZcvd catalyst was identified as the best catalyst among those employed in this study. Hence, the characterizations were conducted with mainly the HZcvd catalyst.

3. Results

3.1. Catalyst Performance. The HZcvd catalyst showed much better performance than the HYcvd catalyst in the selective oxidation/ammoxidation of propene.[38] The suitable geometry of the ZSM-5 pore channels and the pentagonal rings

TABLE 1: Performance (Conversions and Selectivities) of ReO_x/Zeolite Catalysts in the Selective Oxidation/Ammoxidation of Propene at 673 K[a]

catalyst	HZ	HZcvd-9.2 (a)[b]	HZcvd-9.2 (b)[b]	HZcvd-9.2 (c)[b]	HZcvd-4.5	HZcvd-1.2	HZimp-4.5	HZphy-9.6	NaZcvd-9.5
Re (wt %)	0.0	9.2	9.2	9.2	4.5	1.2	9.5	9.6	9.5
conversion (%)	19.6	15.6	15.2	3.8	15.0	16.4	20.0	22.0	4.8
selectivity (%)									
(1) cracking	93.2	5.5	5.3	31.8	6.5	9.2	59.0	48.3	6.0
ethene	21.5	0.0	0.0	18.0	0.0	0.0	8.5	10.5	0.0
methylamine	15.0	1.6	1.7	0.0	1.5	1.8	11.2	9.8	0.0
dimethylamine	14.8	1.3	1.2	0.0	1.1	1.4	12.5	8.0	0.0
ethylamine	22.0	2.6	2.4	0.0	3.9	5.2	14.0	10.2	0.0
butene	19.9	0.0	0.0	13.8	0.0	0.8	11.8	9.8	6.0
(2) selective oxidation ammoxidation	0.0	80.3	82.5	0.0	81.6	75.2	7.5	10.2	6.5
acrolein	0.0	61.6	63.0	0.0	63.5	61.0	6.0	6.2	5.5
acrylonitrile	0.0	18.7	19.5	0.0	18.1	14.2	1.5	4.0	1.0
(3) other products	6.8	14.2	12.2	68.2	11.9	15.6	33.5	41.5	87.5
acetonitrile	0.0	4.6	4.2	4.0	3.8	4.8	16.5	20.0	17.5
CO_2	2.0	4.9	4.3	60.0	3.5	5.2	10.0	12.6	68.0
BTX	4.8	4.7	3.7	4.2	4.6	5.6	7.0	8.9	2.0

[a] Reaction conditions: GHSV 19 200 h^{-1}, $C_3H_6/NH_3/O_2/He$ = 7.5/7.5/10.0/75.0%. [b] (a) The HZmto sample was treated in He to form HZcvd, and (b) the HZmto sample was treated in NH_3/He (50/50%) to form HZcvd. (c) The reaction was conducted on catalyst a in the absence of NH_3 ($C_3H_6/O_2/He$ = 7.5/10.0/82.5%).

of the zeolite framework may provide the superiority of the HZcvd catalyst.[43] Hence, we concentrated our attention on the ZSM-5-based catalysts. Performance data of various catalysts in the selective oxidation/ammoxidation of propene are given in Table 1. The obtained products are classified conveniently as three groups, namely, (a) cracking products (ethene, methylamine, ethylamine, dimethylamine, and butene); (b) selective oxidation/ammoxidation products (acrolein and acrylonitrile); and (c) other products (acetonitrile, CO_2, and BTX). The order of the selectivity toward acrolein + acrylonitrile for the various catalysts is as follows: HZcvd-9.2 = HZcvd-4.5 > HZcvd-1.2 > HYcvd-9.0 > HZimp-9.5 ≈ HZphy-9.6 ≈ HYimp-9.6 > NaZcvd-9.5 > HZ ≈ HY. The numbers in the catalyst notations are Re loadings in wt %. Among these catalysts, the highest selectivity (80.3%) of acrolein + acrylonitrile at the 15.6% conversion of propene at 673 K was achieved with HZcvd-9.2. Contribution of ReO_x species can be understood by comparing the catalytic performance of HZcvd and HZ. Neither acrolein nor acrylonitrile was produced on HZ, where cracking selectivity (93.2%) mainly proceeded. We note that the cracking activity of HZ was suppressed by the incorporation of ReO_x in HZ. Similarly, propene was cracked into many products (95.5%) on HY, whereas the Re-containing HY zeolite (HYcvd) exhibited 46% selectivity toward acrolein + acrylonitrile as the main product.[37]

The role of the proton sites of the zeolites in the catalytic performance was investigated by comparing the product distributions over HZcvd-9.2 and NaZcvd-9.5. The HZcvd-9.2 catalyst exhibited 80.3% selectivity toward acrolein + acrylonitrile against 6.5% selectivity for NaZcvd-9.5, as shown in Table 1. Complete oxidation to CO_2 mainly proceeded on the NaZcvd-9.5 catalyst. HZimp-9.5 and HZphy-9.6 exhibited very low activities toward acrolein + acrylonitrile (7.5 and 10.2% selectivity, respectively) (Table 1). On these catalysts, cracking (59 and 51.7%, respectively) reactions were predominant. Hence, the CVD process in the presence of HZ protons may provide an efficient active site.

To know the effect of Re loading on the selectivity toward acrolein + acrylonitrile, we compared the performance of HZcvd-9.2, HZcvd-4.5, and HZcvd-1.2 (Table 1). The selectivities of these catalysts were 80.3, 81.6%, and 75.2%, respectively.

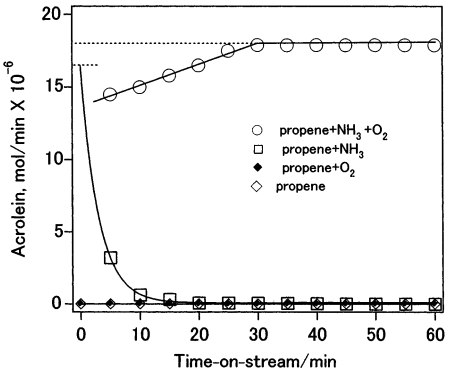

Figure 1. Influence of various reactant compositions on the propene-selective oxidation of HZcvd-9.2: ○, propene/NH_3/O_2/He = 7.5/7.5/10.0/75.0%; □, propene/NH_3/He = 7.5/7.5/85.0%; ◆, propene/O_2/He = 7.5/10.0/82.5%; ◇, propene/He = 7.5/92.5%. GHSV = 19 200 h^{-1}. catalyst weight = 100 mg.

The low selectivity of HZcvd-1.2 accompanied by the relatively higher cracking activity can be ascribed to the availability of free protons.

It was found that ammonia played a decisive role in the selective oxidation of propene to acrolein as shown in Table 1. It is obvious that no selective oxidation occurred in the absence of ammonia. The coexistence of ammonia was a prerequisite for the catalyst performance.

To understand this aspect, the performance of the HZcvd catalyst was studied at various reactant compositions (Figure 1) such as propene + O_2, propene + NH_3, propene + O_2 + NH_3 steady state, and propene alone. The catalyst could not convert propene to acrolein under propene alone and propene + O_2 in the absence of ammonia. However, the catalyst produced acrolein at the beginning of the reaction under propene + NH_3 in the absence of oxygen, and the activity rapidly declined with time. Better catalyst performance with good activity and time-on-stream stability was observed in the steady-state condition of propene + NH_3 + O_2. The extrapolation of the time profile for propene + NH_3 to time zero by exponential fitting showed a rate of 1.65×10^{-5} mol/min, which was similar to the steady-state ratio of 1.79×10^{-5} mol/min for acrolein formation.

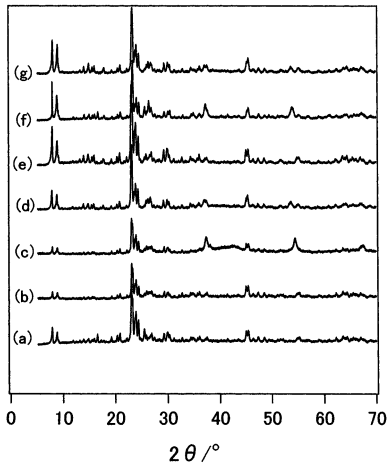

Figure 2. X-ray diffraction patterns for (a) HZcvd-1.2, (b) HZcvd-4.5, (c) HZcvd-9.2, (d) HZrct(4)-9.2, (e) HZphy-9.6, (f) HZimp-9.5, and (g) NaZcvd-9.5.

This indicates that the lattice oxygen of the HZcvd catalyst contributes to the formation of acrolein in the initial stage of the reaction. The total amount of acrolein formed in 10 min in the absence of ammonia corresponds to about 70% of the Re quantitatively in the catalyst.

3.2. Catalyst Characterization.

3.2.1. XRD. XRD patterns for the various ReO_x/zeolite samples are shown in Figure 2. A part of Figure 2 was reported in the previous paper.[38] All of the samples exhibited the characteristic patterns of the ZSM-5 structure, but there are differences in intensities of some peaks. The following changes in XRD for HZmto-9.2 and HZcvd-9.2 samples were observed in Figure 2: (1) the intensity of the peaks at $2\theta = 6.4-10°$ decreased, which indicates an increase in the amount of adsorbed water (hydrophilic nature of zeolite);[44,45] (2) the intensity of the doublet at 44.5−46° decreased (decrease in the framework Si/Al ratio);[46] and (3) the intensity of the peaks at 22.5−24.0° decreased (decrease in zeolite crystallinity).[47] However, the intensities of the peaks at 6.4−10°, 22.5−24.0°, and 44.5−46° increased after the NH_3 treatment and the catalytic reaction (HZ_{NH_3}-9.2 and HZrct(2)-9.2). This means that a recovery of the decreased crystallinity of the H-ZSM-5 framework occurred during the NH_3 treatment and the catalytic reaction. Unlike HZcvd-9.2, for HZphy-9.6 and HZimp-9.5, the characteristic peaks reflecting crystallinity and hydrophilicity remained unchanged. NaZcvd-9.5 did not exhibit any changes in XRD patterns that were responsible for changes in crystallinity and hydrophilicity either. The phenomenon of the framework change was observed only in the case of the HZcvd sample. A small amount of ReO_2 (XRD peaks around 37.5 and 56°) was formed for HZcvd-9.2, but ReO_2 was not observed for HZrct(6)-9.2 (after six reaction runs).

3.2.2. Solid-State ^{29}Si MAS NMR. Deconvoluted ^{29}Si MAS NMR spectra for ReO_x/HZ samples are given in Figure 3. HZ exhibits a peak at about −106 ppm and a doublet at −112 and −116 ppm; these are assigned to Si(1-Al), Si(0-Al)$_5$, and Si(0-Al)$_4$ respectively.[48] Si(0-Al)$_5$ and Si(0-Al)$_4$ indicate Si atoms in the five- and four-membered rings of ZSM-5, respectively. Changes in the intensities of the peaks were observed after Re incorporation, as shown in Table 2. The intensity of Si(1-Al) increased from 0.183 (HZ) to 0.363 (HZmto-9.2), and that of Si(0-Al) decreased from 0.817 (HZ) to 0.637 (HZmto-9.2) after the CVD of MTO to HZ (HZmto-9.2). A chemical shift from −106 to −108 ppm was also observed for Si(1-Al) in HZmto-9.2. These changes resulted in the decrease in the Si/Al of the sample from 20.11 (HZ) to 11.03 (HZmto-9.2). No significant change in the intensity was observed in HZphy-9.5 (Table 2). On the contrary, a considerable decrease in Si(1-Al) from 0.183 to 0.083 and an increase in Si(0-Al) from 0.817 to 0.917 occurred for HZimp-9.5, which indicates the occurrence of significant dealumination and framework destruction of H-ZSM-5.

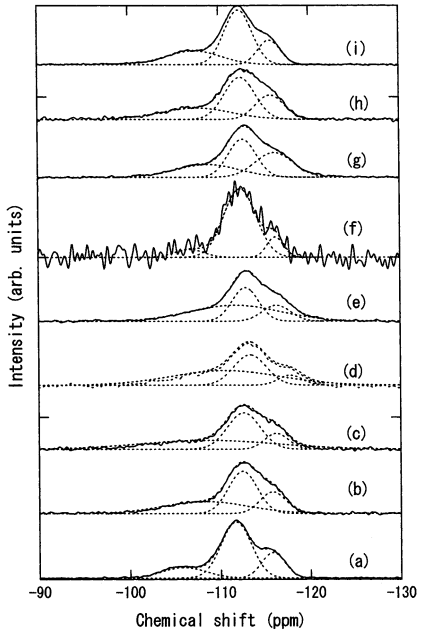

Figure 3. ^{29}Si MAS NMR spectra for (a) HZ, (b) HZmto-9.2, (c) HZcvd-9.2, (d) HZ_{NH_3}-9.2, (e) HZrct(2)-9.2, (f) HZimp-9.5, (g) HZphy-9.6, (h) HZmto-4.5, and (i) HZmto-1.2. Dotted lines indicate deconvoluted peaks.

The ^{29}Si NMR spectra of HZcvd-1.2, HZcvd-4.5, and HZcvd-9.2 containing 1.2, 4.5, and 9.2 wt % Re, respectively, are shown in Figure 3. Irrespective of the amount of Re loaded, the phenomena of increase in Si(1-Al) and decrease in Si(0-Al) were observed as given in Table 2.

3.2.3. Solid-State ^{27}Al MAS NMR. In situ ^{27}Al NMR spectra for samples sealed under vacuum were measured without exposure to air (Figure 4a). The peak near 55 ppm indicates the presence of tetrahedral (framework) Al.[49] There was a change in the intensity and position of the peak. For HZmto and HZcvd, the peak became broad and shifted to 50 ppm. This indicates a strong electric field around the framework alumina in these samples. Interestingly, the peak came back to its original position around 55 ppm after the ammonia treatment (HZ_{NH_3}) and the catalytic reaction (Figure 4a−e).

Ex situ ^{27}Al NMR spectra were also measured (Figure 4b), where HZ, HZmto, HZcvd, HZ_{NH_3}, and HZrct were exposed to moisture. HZ exhibited only one peak around 60 ppm due to tetrahedral (framework) Al. A peak around 0 ppm due to octahedral Al appeared after CVD of MTO (HZmto) (Figure 4b−b). The intensity increased after the pretreatment at 673 K (HZcvd) (Figure 4b−c). The peak for octahedral Al disappeared after NH_3 treatment (HZ_{NH_3}) and the catalytic reaction (HZrct). The ex situ ^{27}Al NMR spectra for HZ, HZ_{NH_3}, and HZrct were similar to the in situ ^{27}Al NMR spectra, whereas the ex situ spectra for HZmto and HZcvd were different from the in situ spectra. This means that a part of Al in HZmto and HZcvd possess hydrophilic character compared to that of the Al atoms in HZ, HZ_{NH_3}, and HZrct.

^{27}Al MAS NMR spectra were also measured for CVD samples with different Re loadings: 1.2, 4.5, and 9.2 wt %

TABLE 2: Summary of ^{29}Si and ^{27}Al MAS NMR Data for Various Samples

	^{29}Si NMR										^{27}Al NMR					
	Si(1Al)			Si(0Al) five-member			Si(0Al) four-member				Al(tet)			Al(oct)		
sample	δ(ppm)	fwhm	intensity[a]	δ(ppm)	fwhm	intensity[a]	δ(ppm)	fwhm	intensity[a]	Si/Al	δ(ppm)	fwhm	intensity[a]	δ(ppm)	fwhm	intensity[a]
HZ	−105.9	4.9	0.183	−111.7	3.4	0.603	−115.8	2.6	0.214	21.88	52.9	11.7	1.000	–		
HZcvd-1.2	−109.1	10.6	0.319	−112.3	3.0	0.477	−115.7	2.7	0.204	12.56	53.7	8.6	0.758	−0.3	7.8	0.242
HZcvd-4.5	−108.4	9.5	0.351	−112.2	3.2	0.460	−115.7	2.8	0.189	11.39	53.7	9.5	0.796	−1.1	8.1	0.204
HZmto-9.2	−108.3	9.5	0.363	−112.5	3.2	0.436	−115.8	2.9	0.201	11.03	51.5	12.8	0.775	−0.5	8.4	0.225
HZcvd-9.2	−108.6	15.2	0.436	−112.6	3.7	0.429	−116.2	2.7	0.135	9.17	52.4	10.0	0.626	−1.6	6.1	0.374
HZ_{NH_3}−1.2	−110.6	11.9	0.562	−113.3	3.6	0.354	−117.8	2.6	0.084	7.12	50.7	10.0	1.000			
HZrct(2)−9.2	−111.7	10.0	0.519	−112.8	3.0	0.320	−116.3	3.1	0.162	7.71	51.7	9.5	1.000			
HZimp-9.5	−106.7	3.2	0.083	−112.3	3.6	0.797	−116.2	1.8	0.120	48.35	54.0	8.1	0.931	−0.7	5.0	0.069
HZphy-9.6	−108.8	7.0	0.287	−112.6	3.1	0.379	−116.2	4.2	0.335	13.95	51.5	10.0	1.000			
NaZcvd-9.5	−107.2	7.5	0.434	−111.5	3.2	0.267	−114.1	4.3	0.299	9.21	53.7	9.2	0.947	−1.6	7.8	0.053

[a] Peak area (arbitrary units).

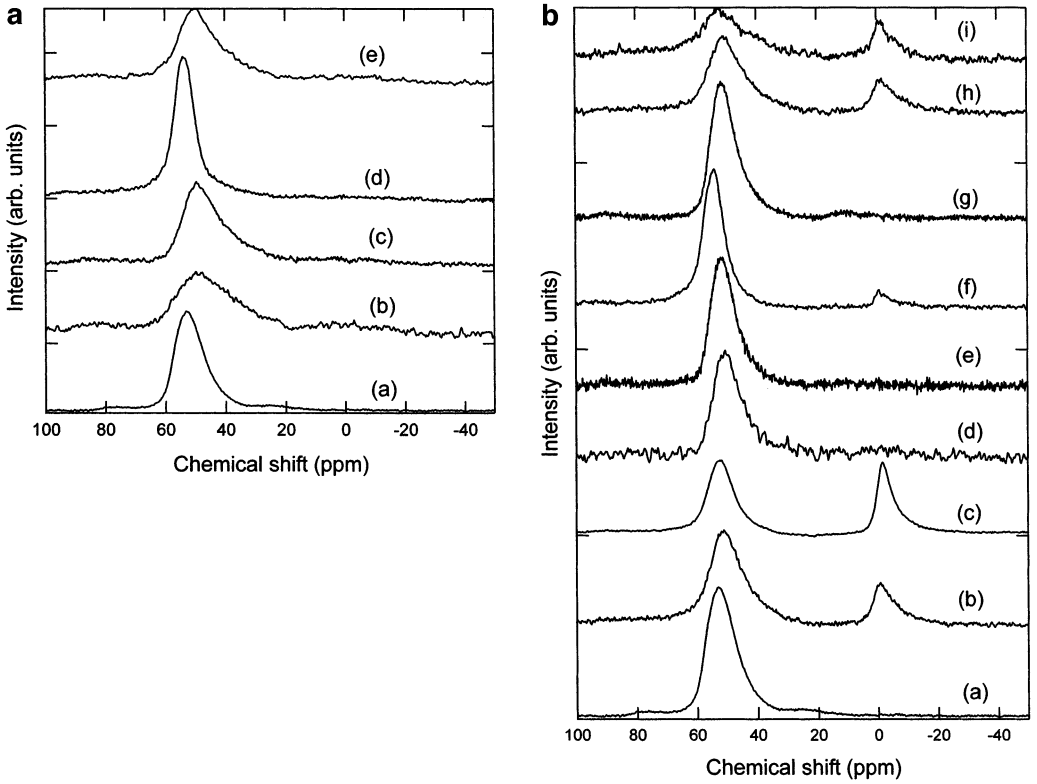

Figure 4. (a) In situ ^{27}Al MAS NMR spectra for (a) HZ, (b) HZmto-9.2, (c) HZcvd-9.2, (d) HZ_{NH_3}-9.2, and (e) $HZ_{(C_3^=+O_2)}$-9.2. (b) Ex situ ^{27}Al MAS NMR spectra for (a) HZ, (b) HZmto-9.2, (c) HZcvd-9.2, (d) HZ_{NH_3}-9.2, (e) HZrct(2)-9.2, (f) HZimp-9.5, (g) HZphy-9.6, (h) HZmto-4.5, and (i) HZmto-1.2.

(Figure 4b). The amount of octahedral Al increased with Re loading—20% Al_{oct} for 1.2 wt % Re and 37% Al_{oct} for 9.2 wt % Re—but the degree of increase was not proportional to the Re loading.

3.2.4. EXAFS and XANES. Figure 5 shows Re L_I-edge XANES spectra of the reference compounds (ReO_2, ReO_3, and Re_2O_7) and several ReO_x/HZ samples obtained by sequential treatments (HZmto, HZcvd, HZ_{NH_3}, and HZrct). A preedge peak at 12 535 eV was observed for Re_2O_7, HZmto-4.5, HZcvd-4.5, HZmto-1.2, HZ-cvd-1.2, and $HZ_{C3}{=}_{+O2}$-1.2 samples. The preedge peak is characteristic of tetrahedral [ReO_4] structure.[44] The preedge peak was not observed definitely after ammonia treatment (HZ_{NH_3}) and exposure of the HZ_{NH_3} to propene + O_2 at 673 K. The structural change in the ReO_x species is indicated with these samples. We conclude that the ReO_x species in HZmto, HZcvd, and $HZ_{C_3^=+O_2}$-1.2 possess a tetrahedral structure symmetry but that ammonia induces a structural change at 673 K. The change is reversible, and the tetrahedral structure is recovered by treatment with oxygen in the absence of ammonia.

Figure 6a and b shows Fourier-transformed EXAFS functions ($k^3\chi(k)$) at the Re L_{111} edge together with curve-fitting results for the Re/HZSM-5 samples. Table 3 summarizes the structural parameters for the Re/H-ZSM-5 samples delivered by the curve-fitting analysis. The small residual factors (R_f) in the EXAFS analyses for the ReO_x/HZ samples indicate that the fitting has been done properly. After MTO exposure to HZ, Re−O and/or Re−C contributions were observed at 0.171 and 0.201 nm with coordination numbers (CNs) of 3.0 and 1.1, respectively, as shown in Table 3. The Re−O and Re−C distances in CH_3-ReO_3 (MTO) are 0.171 and 0.201 nm, respectively. Thus, the EXAFS analysis results demonstrate that MTO retained the structure after the CVD of MTO at 333 K.

When the HZmto (1.2 wt % Re) sample was heated in He at 673 K (HZcvd catalyst), one shell (Re−O) fitting reproduced the observed EXAFS data. The Re−O distance and CN were determined to be 0.17 nm and 4.4, respectively. However, at the higher Re loading (HZcvd-4.5), the presence of ReO_2 with characteristic Re−O bonds around 0.2 nm and Re−Re bonds

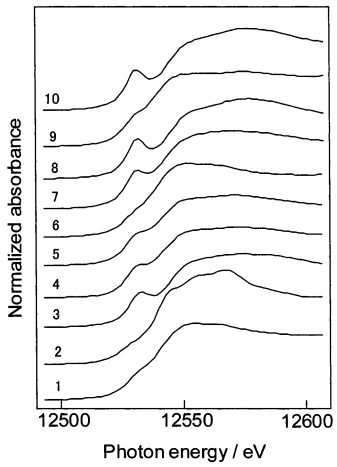

Figure 5. Re L_1-edge XANES spectra for Re/H-ZSM-5 samples and reference oxides: (1) ReO_2, (2) ReO_3, (3) Re_2O_7, (4) HZmto-4.5, (5) HZcvd-4.5, (6) HZrct(2)-4.5, (7) HZmto-1.2, (8) HZcvd-1.2, (9) HZ_{NH_3}-1.2, and (10) $HZ_{(C_3^=+O_2)}$-1.2.

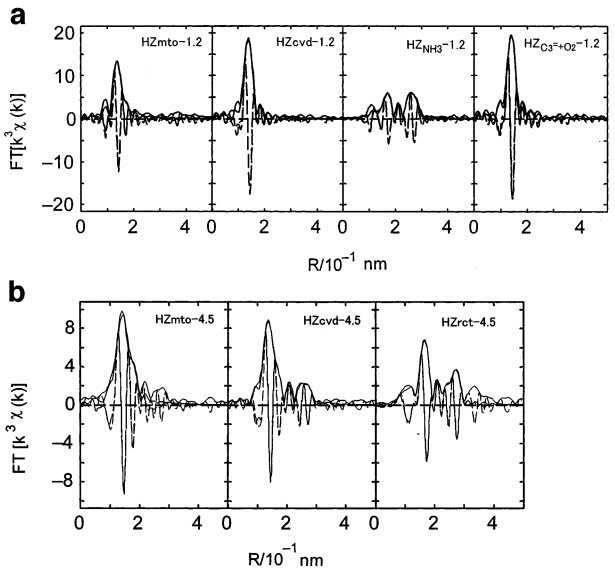

Figure 6. (a) Fourier-transformed k^3-weighted EXAFS functions for HZmto-1.2, HZcvd-1.2, HZ_{NH_3}-1.2, and $HZ_{(C_3^=+O_2)}$-1.2. (b) Fourier-transformed k^3-weighted EXAFS functions for HZmto-4.5, HZcvd-4.5, and HZrct(2)-4.5. Solid and dashed lines indicate experimental and calculated data, respectively.

around 0.26 nm was also indicated (Figure 6b). However, a preedge peak at 12 535 eV in the L_I-edge XANES spectrum indicates that the main species in HZcvd-4.5 is a tetrahedral [ReO_4] species. The EXAFS analysis for HZcvd-4.5 was successfully performed in Table 3, which shows the formation of a tetrahedral [ReO_4] species with a Re−O distance of 0.172 nm (CN = 4.4) during the treatment of HZmto-4.5 at 673 K for 4 h.

Ammonia treatment caused a significant change in the ReO_x species. When the HZcvd-1.2 sample was exposed to NH_3 at 673 K (HZ_{NH_3}-1.2), two different Re−O bondings were observed at 0.172 and 0.203 nm. Also, a new Re−Re contribution was observed at 0.276 nm. The observation of Re−Re bonds indicates the formation of ReO_x clusters. The structural parameters are entirely different from those for ReO_2 (Re−O = 0.194 nm (CN = 4), Re−O = 0.211 nm (CN = 2), Re−Re = 0.261 nm (CN = 2), Re−O = 0.312 nm (CN = 2) by XRD crystallography). The phenomenon of ReO_x cluster formation was also observed under catalytic selective oxidation in the presence of NH_3 on HZcvd-4.5 (HZrct-4.5) (Figure 6b and Table 3). At the higher Re loading, the presence of Re−Si bonding was indicated in addition to Re−Re bonding, as shown in Table 3.

TABLE 3: Structural Parameters Delivered by EXAFS Curve-Fitting Analysis for HZmto-1.2, HZcvd-1.2, HZ_{NH_3}-1.2, and HZ_{NH_3}-1.2 Exposed to Propene + O_2 at 673 K

sample and shell	CN	R/0.1 nm	$\sigma^2/10^{-4}$ nm^2	ΔE_0/eV	R_f (%)
HZmto-1.2					
Re−O	3.0 ± 0.5	1.71 ± 0.03	0.2 ± 1.0	8 ± 12	0.6
Re−C	1.1 ± 0.9	2.01 ± 0.03	3.1 ± 2.2		
HZcvd-1.2					
Re−O	4.4 ± 0.6	1.72 ± 0.006	2.0 ± 0.6	12 ± 2	1.8
HZ_{NH_3}-1.2					
Re−O	2.3 ± 1.3	1.72 ± 0.02	11 ± 6.0	11 ± 2	2.8
Re−O	1.8 ± 0.6	2.03 ± 0.01	1.0 ± 1.0		
Re−Re	3.9 ± 0.9	2.76 ± 0.008	6.0 ± 1.0		
HZ_{NH_3}-1.2 exposed to C_3^{2-} + O_2					
Re−O	3.9 ± 0.4	1.73 ± 0.004	0.8 ± 0.5	13 ± 2	0.9
HZmto-4.5					
Re−O	3.0 ± 0.5	1.71 ± 0.03	0.2 ± 1.0	8 ± 12	0.6
Re−C	1.1 ± 0.9	2.01 ± 0.03	3.1 ± 2.2		
HZcvd-4.5					
Re−O	4.4 ± 0.6	1.72 ± 0.006	2.0 ± 0.6	12 ± 2	1.8
HZrct(2)−4.5					
Re−O	0.9 ± 0.3	1.77± 0.01	4[a]	9 ± 2	2.3
Re−O	3.1 ± 0.3	1.99 ± 0.01	4[a]		
Re−Si	1.2 ± 0.7	2.73 ± 0.02	7[a]		
Re−Re	3.3 ± 0.4	2.77 ± 0.01	7.0± 5.0		

[a] Fixed.

Further treatment of HZ_{NH_3}-1.2 with a mixture of propene and O_2 in the absence of ammonia ($HZ_{C_3^=+O_2}$-1.2) exhibited the reformation of tetrahedral [ReO_4] species (Figure 6a and Table 3). The Re−O distance and CN were 1.73 nm and 3.9, respectively, which are similar to those for HZcvd-1.2.

4. Discussion

4.1. Catalyst Performance. The HZcvd-9.2 catalyst prepared by CVD of MTO on HZ at 333 K followed by treatment at 673 K in He exhibited as high as 80.3% selectivity (673 K) to acrolein (main) + acrylonitrile (minor).[38] However, the impregnated (HZimp) and physical mixing (HZphy) catalysts showed much worse performance, 7.5 and 10.2% selectivities, respectively (Table 1). The CVD method seems to be effective for the creation of active sites in H-ZSM-5. HZ alone exhibited 93% cracking selectivity without acrolein formation. Thus, rhenium encapsulation is responsible for the shift in selectivity from cracking to selective oxidation.[38] When NaZ was used as a support, the selectivity toward acrolein + acrylonitrile was as low as 6.5% (Table 1). The NaZcvd-9.5 catalyst was active for combustion to CO_2 (68.0% selectivity). Protons in HZ are believed to be necessary for the formation of active Re species in the CVD process.[38] We note that ammonia showed a significant influence on catalytic performance. No selective oxidation of propene to acrolein proceeded in the absence of ammonia (Table 1). To understand the promoting role of ammonia, structural changes of the ReO_x species in the HZcvd catalysts after the CVD process, NH_3 treatment, and catalytic reactions were investigated with the help of various characterization techniques.

4.2. Active Structure of HZcvd for Selective Oxidation/Ammoxidation of Propene. The following three changes in

SCHEME 1: Structural Changes in the HZcvd Catalyst Preparation and the Catalytic Reaction Conditions

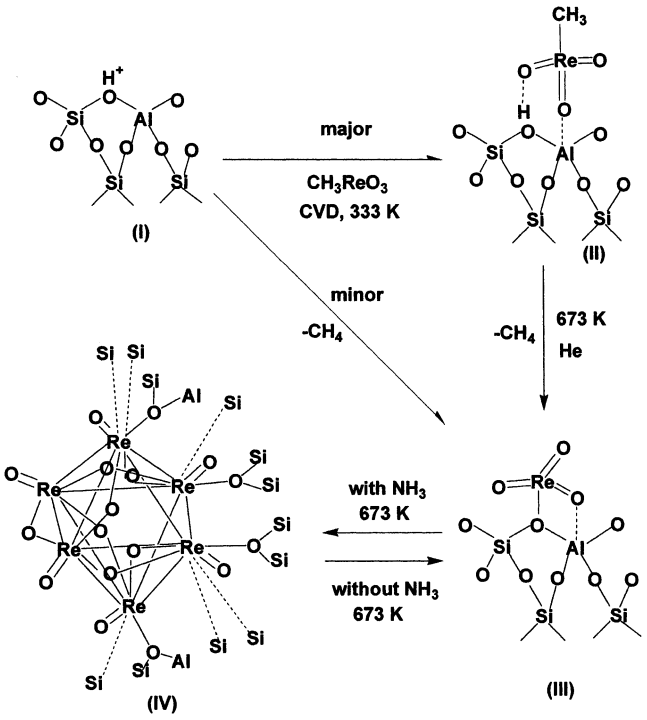

the XRD patterns of Figure 2 were observed for the HZcvd samples: (1) a decrease in the intensity of the peaks at $2\theta = 6.4-10.4°$, (2) a decrease in the intensity of the peaks at 22.5−24.0°, and (3) a decrease in the intensity of the doublet at 44.5−46°. All of these changes suggest a decrease in Si/Al of the ZSM-5 framework and a small decrease in the zeolite crystallinity during the catalyst preparation. Such changes were not observed for the other samples, HZphy and HZimp, where the characteristic peaks reflecting Si/Al and the crystallinity remained almost unchanged.

A part of the XRD patterns in Figure 2 indicate the formation of a small amount of ReO_2, but it was concluded that ReO_2 was not the active species for the selective oxidation/ammoxidation.[38] Furthermore, the HZcvd-1.2 catalyst shows no XRD peaks for ReO_2 (Figure 2), whereas it exhibits comparable activity (75.2% selectivity) to that of HZcvd-9.2 (80.3% selectivity) (Table 1).

A schematic illustration for the HZcvd catalyst and the active ReO_x cluster is shown in Scheme 1, which can explain the structural changes in the zeolite framework and the ReO_x species in the successive steps such as the MTO CVD at 333 K, the treatment at 673 K, the NH_3 treatment at 673 K, and the propene + O_2 treatment at 673 K. The Re L_{III}-edge EXAFS structural analyses for HZmto-1.2 and HZmto-4.5 show that the MTO encapsulated in HZ retains its structural integrity with no significant distortion compared to the structure of bulk MTO (Re−C = 0.206 ± 0.01 nm with CN = 1, Re−O = 0.174 ± 0.003 nm with CN = 3). The corresponding values for gaseous MTO are Re−C = 0.2060 nm and Re−O = 0.1709 nm.[50] The IR spectrum of HZ exhibited a peak at 3610 cm^{-1} due to zeolitic protons, and its intensity decreased significantly after the MTO CVD at 333 K (HZmto-9.2), which suggests that the majority of the protons interacted with MTO. This is in agreement with the results for MTO encapsulated in HY.[51] The interaction can be considered to be hydrogen bonding between an oxo ligand of MTO and a proton of HZ, as shown in Scheme 1.

Because bulk MTO decomposes at 523 K, the treatment of HZmto at 673 K in He is expected to cause the decomposition of the MTO in HZ to form ReO_x. CH_4 was evolved during the treatment at 673 K. The amount of CH_4 evolved was 80% of the MTO in HZ. This confirms that the encapsulation of the majority of MTO in HZ occurs without decomposition at 333 K. The HZcvd catalyst after the treatment at 673 K is shown as in structure III in Scheme 1. Structure III constitutes [ReO_4] monomers in a tetrahedral symmetry, as proved by XANES at the Re L_1 edge and EXAFS at the Re L_{111} edge (Figures 5 and 6). The Re−O bonds in the tetrahedral [ReO_4] monomer were 0.172 nm irrespective of Re loadings (1.2 and 4.5 wt %), as shown in Table 3. The bonding of the hydrophilic [ReO_3] moiety to the Si−O−Al bridge oxygen may increase the hydrophylic nature of HZ. Indeed, the increased hydrophilic nature of the HZ zeolite was suggested from the XRD data in Figure 2 for HZmto and HZcvd, where the peak intensities at 6.4−10.4° decreased because of more adsorbed water.

The ex situ ^{27}Al NMR spectra for HZ exposed to air with moisture (Figure 4b) showed no octahedral Al (Al_{oct}), but Al_{oct} was observed for HZmto and HZcvd samples exposed to air with moisture (Figure 4b). However, no Al_{oct} was observed in the in situ ^{27}Al NMR measurements of these samples (Figure 4a) because there was no water adsorption under the in situ conditions. However, there was a shift in the peak position of the tetrahedral Al (Al_{tet}) from 60 to 50 ppm (Figure 4a). The shifts increase with electron shielding around the Al_{tet}. Increased electron shielding in these samples can be explained by the additional bonding between [ReO_3] and Al_{tet} (structures II and III in Scheme 1).

The HZcvd catalyst with structure III was used in the selective oxidation/ammoxidation of propene. Unlike the cases of HZmto and HZcvd, no Al_{oct} was observed in the ex situ ^{27}Al NMR spectrum for HZ_{NH_3} (Figure 4b). The in situ ^{27}Al MAS spectrum for HZ_{NH_3} is also different from those for HZmto and HZcvd (Figure 4a). The peak shifted back to its original position from 50 to 60 ppm after the NH_3 exposure at 673 K (HZ_{NH_3}). The ^{27}Al NMR results indicated that the additional interaction between MTO and Al_{tet} disappeared because of the NH_3 exposure. The L_1-edge XANES spectra in Figure 5 also changed after the NH_3 exposure (HZ_{NH_3}-1.2) and the catalytic reaction (HZrct-4.5). The structural parameters delivered by the EXAFS curve-fitting analysis of EXAFS (Table 3) revealed significant changes in the coordination environment of Re atoms after the NH_3 exposure and the catalytic selective oxidation/ammoxidation reaction.

After the ammonia treatment, the EXAFS functions for HZ_{NH_3}-1.2 drastically changed. The new Re−Re bond at a distance of 0.276 nm appeared, and the coordination number (CN) was 3.9 (±0.4), as shown in Table 3. In addition, two types of Re−O bonds were observed at 0.172 and 0.203 nm; the shorter bonds are attributed to Re═O, and the longer ones may be attributable to Re-O_{bridge} and/or Re−$O_{lattice}$. The EXAFS analysis indicates the formation of a ReO_x cluster. Values of 0.276 nm for Re−Re and 3.9 for CN indicate an octahedral cluster (Re_6) framework with direct Re−Re bonding. We propose a cluster structure in Figure 7.

The cluster structure is composed of a Re_6O_{13} cluster moiety that is bound to four oxygen atoms of the zeolite framework, and the overall cluster formulation is described as Re_6O_{17}. The cluster contains six Re atoms in octahedral geometry (Re−Re = 0.276 nm), and the Re atoms occupy six corners of the octahedron. Thus, each Re atom is four-coordinated with neighboring Re atoms, which coincides with the CN of 3.9

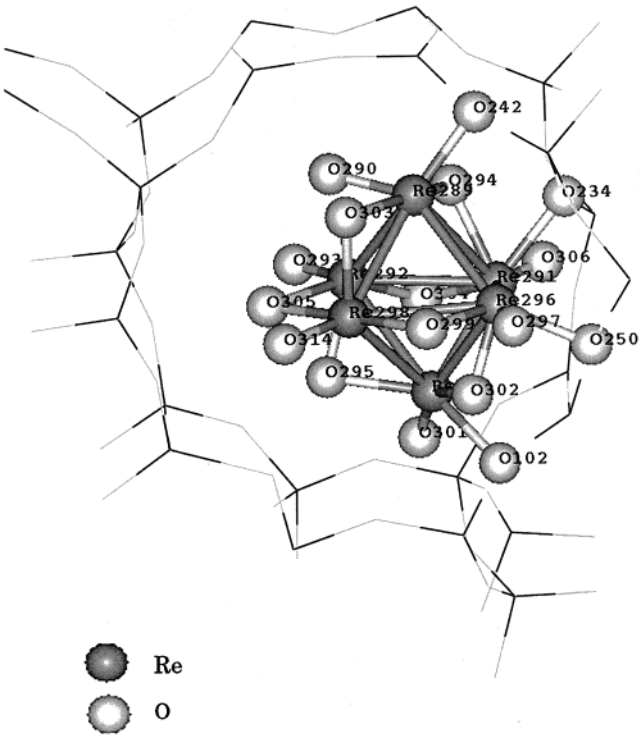

Figure 7. Proposed structure of active $[Re_6O_{17}]$ cluster in the ZSM-5 pore channel, where the $[Re_6O_{17}]$ cluster is bound to the pentagonal rings of the zeolite inner wall.

determined by EXAFS. The detailed EXAFS analysis for the HZrct-4.5 catalyst with 4.5% Re loading revealed the Re−Si contribution at 0.273 nm (CN = 1.2 ± 0.7) in addition to the Re−Re bonding at 0.277 nm (CN = 3.3 ± 0.4), as shown in Table 3. The $[ReO_4]$ monomers were bound to the Si−O−Al (H^+ position) oxygen of the zeolite framework. Thus, we put the Re_6 cluster at the position where the geometric arrangement of the Re_6 cluster fits in with the location of the Si−O−Al oxygen atoms as well as the distance from the Si atoms of the HZ framework, assuming C_2 symmetry. The cluster was located 0.2 nm from the zeolite wall, four rhenium atoms were located near the side of the zeolite wall, and each of the four Re atoms connected with one zeolite oxygen atom (Re−O ≈ 0.2 nm). The other two Re atoms located at the center of the channel were free from any interactions with the zeolite framework. The treatment with NH_3 at 673 K reduces the Re^{7+} oxidation state of structure III in Scheme 1 to the lower valence levels, which is supported by the CNs of Re═O and Re−O in Table 3. However, the structural parameters determined by the EXAFS analysis in Table 3 are entirely different from those for ReO_3 (Re−O = 0.187 nm (CN = 6) and Re−Re = 0.373 nm (CN = 6) by X-ray crystallography). ReO_2 was not active for the selective oxidation/ammoxidation of propene, and the structural parameters for ReO_2 are also entirely different from those for the Re_6 cluster, as mentioned above. Hence, the oxidation state of Re in the cluster may be Re^{5+} or Re^{6+} (which is different from that of ReO_3) or a mixture of Re^{5+} and Re^{6+}. Oxygen atoms were coordinated to the Re_6-cluster framework in such a way that each Re atom possessed a similar coordination environment (CN < 8) around each Re atom. We could not find any reasonable coordination structure where the oxidation state of all of the Re atoms was 5+ or 6+. We have found the most plausible structure on the basis of a mixture of Re^{5+} and Re^{6+}, as illustrated in Figure 7. There are six terminal and seven bridging oxygen atoms in the cluster, where each Re atom bears one terminal oxygen atom (Re═O = 0.172 nm). Rhenium atoms in the cluster are also coordinated with seven bridging oxygen atoms. As consequence, each Re atom is coordinated with one terminal oxygen and three bridging oxygen atoms. Quantitative temperature-programmed reduction (TPR) may provide the average oxidation state of the Re.[52] FTIR spectra for the catalyst indicated the presence of NH species under the reaction conditions, but the quantity was small and could not be determined. A small part of the bridging oxygens in the cluster might be replaced by NH. A preliminary calculation by density functional theory (DFT) was conducted to examine whether the proposed structure of Figure 7 was reasonable energetically. The calculation was done by fixing the Re_6 octahedral framework and the Re−O bondings at the interface, where only the arrangement of 13 oxygen atoms was optimized as a free parameter. The oxygen coordination structure of Figure 7 was compatible with the DFT calculation. The proposed Re_6O_{17} cluster with terminal and bridging oxygen atoms may explain the bifunctional catalysis for the propene-selective oxidation, where both allylic C−H bond scission and oxygen incorporation processes are involved. When the HZ_{NH_3}-1.2 sample was allowed to react with a mixture of propene and oxygen, the Re_6O_{17} cluster was transformed back to the original $[ReO_4]$ monomers, as shown in Figure 6a and Table 3.

Chen et al. reported a reversible transformation between Fe ions and small iron oxide clusters in MFI containing Fe ions by FTIR.[53] When the Fe/MFI sample is treated with aqueous NaOH, small iron oxide clusters are generated, whereas Fe ions are regenerated upon replacing Na^+ by H^+ ions and initiating protonolysis at high temperature. This may be analogous to the reversible transformation of ReO_x species in our system. However, ReO_2 particles were formed on NaZ_{CVD} and were inactive for selective oxidation/ammoxidaton.[38]

4.3. Interaction of Rhenium Species with Si(0-Al)$_5$. The ^{29}Si NMR peak intensity for Si(1-Al) increased by CVD of MTO at 333 K, whereas that for Si(0-Al) decreased in the HZmto-9.2 sample, as shown in Figure 3 and Table 2. We note that the decrease occurred in the ^{29}Si NMR peak of pentagonal ring Si-(0-Al)$_5$ and not in that of four-membered ring Si(0-Al)$_4$. Decreasing Si(0-Al)$_5$ and increasing Si(1-Al) became prominent after the treatment at 673 K (HZcvd). Hence, the Re−pentagonal ring interaction is suggested to occur partly during CVD of MTO and to increase by the treatment of HZmto to form HZcvd. These results demonstrate that the complete decomposition of MTO during the treatment at 673 K facilitates the formation of $[ReO_4]$ species and that the resultant $[ReO_4]$ species interacts with Si-(0-Al)$_5$ of HZ, which is reflected in the decrease in zeolite crystallinity (XRD in Figure 2), the increase in the hydrophilic nature (XRD in Figure 2), the conversion of Si(0-Al)$_5$ to Si(1-Re) (not discriminated from Si(1-Al) in ^{29}Si NMR in Figure 3), and the peak shift in ^{27}Al NMR in Figure 4. All of the data prove the rheniation of the H-ZSM-5 framework (Scheme 1).

The initial interaction of rhenium with protons, followed by the formation of the $[ReO_4]$ species and its interaction with the zeolite framework through Si(0-Al)$_5$, is facilitated efficiently by the CVD method but not by impregnation and physical mixing. The lack of such interaction in HZimp and HZphy cannot facilitate the formation of active rhenium clusters. Similarly, the absence of protons in NaZ can explain the inactivity of NaZcvd for propene-selective oxidation (Table 1).

4.4. Contribution of Lattice Oxygen to the Selective Oxidation. The performance of HZcvd was examined under the condition of propene + NH_3. In the absence of oxygen, acrolein was formed in the initial stage of the reaction, but the produced amount rapidly decreased and reached zero within 20

min (Figure 1). The rate of acrolein formation at zero time was estimated to be 1.65×10^{-5} mol/min from the exponential extrapolation. The value is similar to 1.79×10^{-5} mol/min at the steady state of the reaction. The total amount of acrolein formed in the absence of oxygen was calculated from Figure 1 to be about 70% of the quantity of Re in the catalyst. Hence, 32% of the oxygen atoms in the $[Re_6O_{13}]$ moiety can be considered to be active oxygen for the selective oxidation of propene.

5. Conclusions

5.1. Chemical vapor deposition (CVD) of methyl trioxorhenium (MTO) on H-ZSM-5 (HZ) at 333 K facilitated the molecular-level interaction between rhenium and zeolite protons. The subsequent treatment at 673 K formed tetrahedral $[ReO_4]$ species that were chemically bound to the pentagonal ring (Si-(0-Al)$_5$) of the zeolite.

5.2. The obtained HZcvd catalyst performed well for the selective oxidation/ammoxidation of propene. The existence of ammonia was a prerequisite for the catalytic selective oxidation of propene.

5.3. Ammonia transformed the $[ReO_4]$ monomers to ReO_x clusters, which were active species that were relevant to the catalytic selective oxidation/ammoxidation of propene. Ammonia also stabilized the clusters to prevent them from decomposing to the original monomers under the catalytic reaction conditions.

5.4. A novel $[Re_6O_{17}]$ cluster structure was proposed on the basis of the EXAFS analysis and the preparation steps. The structure is composed of a $[Re_6O_{13}]$ moiety and four framework oxygen atoms of HZ.

5.5. Rhenium atoms in the cluster were coordinated with terminal and bridge oxygen atoms, 32% of which were active for the selective oxidation.

5.6. The $[Re_6O_{17}]$ clusters were transformed back to the $[ReO_4]$ monomers by exposure to oxygen in the absence of ammonia at 673 K.

Acknowledgment. XAFS measurements were carried out with the approval of the Photon Factory Advisory Committee (PAC) (proposal no. 2000G260). N.V. thanks the Japan Society for the Promotion of Science (JSPS) for his postdoctoral fellowship at the University of Tokyo.

References and Notes

(1) Grasselli, R. K. *Catal. Today* **1999**, *49*, 141.
(2) Albonetti, S.; Cavani, F.; Trifiro, F. *Catal. Rev.—Sci. Eng.* **1996**, *38*, 413.
(3) Centi, G.; Trifiro, F.; Ebner, J. R.; Franchetti, V. M. *Chem. Rev.* **1988**, *88*, 55.
(4) Inoue, T.; Asakura, K.; Iwasawa, Y. *J. Catal.* **1998**, *171*, 184.
(5) Inoue, T.; Asakura, K.; Iwasawa, Y. *J. Catal.* **1998**, *171*, 457.
(6) Khodakov, A.; Yang, J.; Su, S.; Iglesia, E.; Bell, A. T. *J. Catal.* **1998**, *177*, 343.
(7) Albonetti, S.; Blanchard, G.; Burttin, P.; Cavani, F.; Masetti, S.; Trifiro, F. *Catal. Today* **1998**, *42*, 283.
(8) Nilsson, S.; Lindblad, T.; Anderson, A. *J. Catal.* **1994**, *148*, 501.
(9) Zanthoff, H.-W.; Buchhloz, S. A. *Catal. Lett.* **1997**, *49*, 213.
(10) Ruth, K.; Kieffer, R.; Burch, R. *J. Catal.* **1998**, *175*, 16.
(11) Centi, G.; Guarnieri, F.; Perathoner, S. *J. Chem. Soc., Faraday Trans.* **1997**, *93*, 3391.
(12) Kim, Y.-C.; Ueda, M.; Moro-oka, Y. *Catal. Today* **1992**, *13*, 673.
(13) Hatano, M.; Kayo, A. European Patent 318,295, 1991.
(14) Katsumoto, K.; Marquis, D. M. U.S. Patent 4,132,670, 1979.
(15) Lin, M. M. *Appl. Catal.* **2001**, *207*, 1.
(16) Grasselli, R. K.; Centi, G.; Trifiro, F. *Appl. Catal.* **1990**, *57*, 149.
(17) Barber, S.; Booth, J.; Pyke, D. R.; Reid, R.; Tilley, R. J. D. *J. Catal.* **1982**, *77*, 180.
(18) Vedrine, J. C.; Coudurier, G.; Ouqour, A.; Pries de Oliveira, P. G.; Volta, J. C. *Catal. Today* **1996**, *28*, 3.
(19) Guttmann, A. T.; Graselli, R. K.; Brazdil, J. F.; Suresh, D. D. U.S. Patent 4,788,319, 1989.
(20) Davenport, W. H.; Kolonitsch, V.; Line, C. H. *Ind. Eng. Chem.* **1968**, *60*, 10.
(21) Blom, R. H.; Kolonitsch, V.; Line, C. H. *Ind. Eng. Chem.* **1962**, *54*, 17.
(22) Holl, J. C.; Moulijn, J. A. *Adv. Catal.* **1975**, *24*, 131.
(23) Kim, D. S.; Wachs, I. E. *J. Catal.* **1993**, *141*, 419.
(24) Bein, T.; Huber, C.; Moller, K.; Wu, C.-G.; Xu, L. *Chem. Mater.* **1997**, *9*, 2252.
(25) Wang, L.; Ohnish, R.; Ichikawa, M. *J. Chem. Soc., Chem. Commun.* **1998**, 1217.
(26) Wang, L.; Ohnish, R.; Ichikawa, M. *Catal. Lett.* **1999**, *62*, 29.
(27) Jehng, J.-M.; Hu, H.; Gao, X.; Wachs, I. E. *Catal Today* **1996**, *28*, 335.
(28) Harrison, W. T. A.; McManus, A. V. P.; Kaminsky, A. P.; Cheetham, A. K. *Chem. Mater.* **1993**, *5*, 1631.
(29) Yuan, Y.; Liu, H.; Imoto, H.; Shido, T.; Iwasawa, Y. *Chem. Lett.* **2000**, 674.
(30) Yuan, Y.; Shido, T.; Iwasawa, Y. *Chem. Commun.* **2000**, 1421.
(31) Yuan, Y.; Liu, H.; Imoto, H.; Shido, T.; Iwasawa, Y. *J. Catal.* **2000**, *195*, 51.
(32) Liu, H.; Gaigneaux, E.-M.; Imoto, H.; Shido, T.; Iwasawa, Y. *Appl. Catal., A* **2000**, *202*, 251.
(33) Liu, H.; Gaigneaux, E.-M.; Imoto, H.; Shido, T.; Iwasawa, Y. *J. Phys. Chem. B* **2000**, *104*, 2033.
(34) Gaigneaux, E.-M.; Liu, H.; Imoto, H.; Shido, T.; Iwasawa, Y. *Top. Catal.* **2000**, *11/12*, 185.
(35) Liu, H.; Shido, T.; Iwasawa, Y. *Chem. Commun.* **2000**, 1881.
(36) Liu, H.; Shido, T.; Iwasawa, Y. *J. Catal.* **2001**, *200*, 69.
(37) Liu, H.; Iwasawa, Y. *J. Phys. Chem. B* **2002**, *106*, 2319.
(38) Viswanadham, N.; Shido, T.; Iwasawa, Y. *Appl. Catal., A* **2001**, *1*, 5674.
(39) Bein, T.; Huber, C.; Moller, K.; Wi, C. G.; Xu, L. Q. *Chem. Mater.* **1997**, *9*, 2252.
(40) Englehardt, G.; Michel, D. *High-Resolution Solid-State NMR of Silicates and Zeolites;* Wiley & Sons: New York, 1987; pp 247, 303.
(41) Stern, E. A.; Newville, M.; Ravel, B.; Yacoby, Y.; Haskel, D. *Physica B* **1995**, *117*, 208.
(42) Stern, E. *Phys. Rev. B* **1993**, *48*, 9825.
(43) Rehr, J.; Albers, R. *Phys. Rev. B* **1990**, *41*, 8139.
(44) Froba, M.; Lochte, K.; Metz, W. *J. Phys. Chem. Solids* **1996**, *57*, 635.
(45) Shubin, A. A.; Zidomirov, G. M.; Yakovlev, A. L.; Van Santen, R. A. *J. Phys.Chem. B* **2001**, *105*, 45928.
(46) Axon, S. A.; Klinowski, J. *Appl. Catal.* **1989**, *56*, L9.
(47) Wilson, S. T.; Lok, B. M. T.; Messina, C. A.; Cannan, T. R.; Flanigen, J. *J. Am. Chem. Soc.* **1982**, *104*, 1146.
(48) Pollack, S. S.; Adkins, J. W.; Wetzel, E. L.; Newbury, D. *Zeolites* **1984**, *4*, 181.
(49) Hardenberg, T. A. J.; Martens, L.; Mesman, P.; Muller, H. C.; Nicolaides, C. P. *Zeolites* **1992**, *12*, 685.
(50) Hermann, W. A.; Kiprof, P.; Rypdal, K.; Tremmel, J.; Blom, R.; Alberto, R.; Behm, J.; Albach, R. W.; Bock, H.; Solouki, B.; Mink, J.; Lichtenberger, D.; Gruhn, N. E. *J. Am. Chem. Soc.* **1991**, *113*, 6527.
(51) Malek, A.; Ozin, G. *Adv. Mater.* **1995**, *7*, 160.
(52) Hilbrig, H.; Michel, C.; Haller, G. L. *J. Phys. Chem.* **1992**, *96*, 9893.
(53) Chen, H.-Y.; Wang, X.; Sachtler, W. M. H. *Phys. Chem. Chem. Phys.* **2000**, *2*, 3083.